Chapter 2

Microwave-assisted rapid synthesis and effect of Organic Functionality on the antimicrobial activity of metal nanoparticles

2.1 Introduction

The use of functional alkoxysilanes such as 3-aminopropyltrimethoxysilane (3-APTMS) and 3-glycidoxypropyltrimethoxysilane (3-GPTMS; scheme 1.) as potential stabilizing and reducing reagents for the synthesis of noble metal nanoparticles, including gold, silver and palladium nanoparticles as well as multi-metallic nanoparticles, has been described (Pandey & Chauhan, 2012; Pandey et al., 2014 a; Pandey & Pandey 2014 b; Pandey & Pandey 2016). 3-APTMS is a hydrophilic compound with micellar activity; 3-GPTMS is a hydrophobic compound that controls the dispersibility of as-made noble metal nanoparticles. All the noble metal cations, including gold, silver, and palladium cations, can be precisely converted into monometallic, bimetallic, or trimetallic nanoparticles through the active role of these functional alkoxysilanes under ambient conditions within 5–14 h (Pandey et al., 2014 a). The process of nanoparticle synthesis may be facilitated using an organic reducing agent such as cyclohexanone or formaldehyde that enables the formation of nanoparticles within 30 minutes to 6 h (Pandey & Chauhan, 2012; Pandey et al., 2014 a; Pandey & Pandey, 2014 b). This approach controls the dispersibility of the noble metal nanoparticles in various solvents. Since the alkoxysilane and the organic reducing agent are active under microwave processing, the rate of nanoparticle synthesis may be accelerated by microwave processing of a reaction mixture containing noble metal cations or a mixture of noble metal cations. Noble metal nanoparticles and their bi-or tri-metallic analogs can be made within 15–40 s when the 3-

APTMS capped noble metal cations undergo microwave processing in the presence of small organic reducing agents (e.g., cyclohexanone, formaldehyde, and 3-GPTMS).

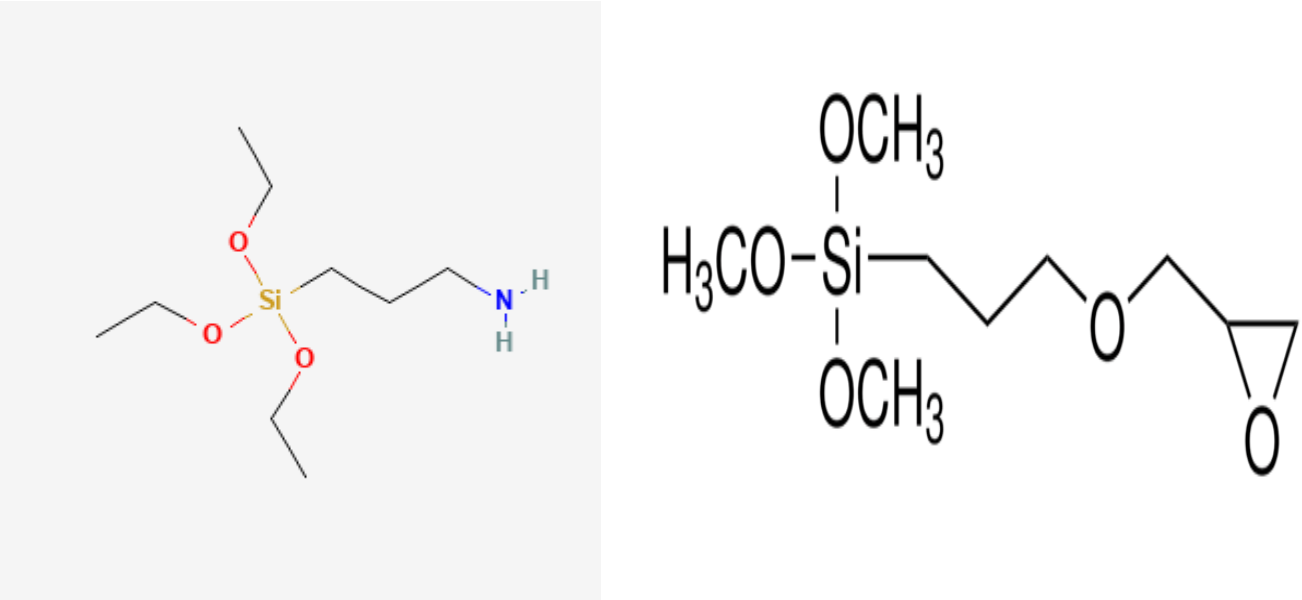

Scheme 2.1 Chemical structure of 3-APTMS and 3-GPTMS.

Over the past few decades, using nanotechnology-based solutions to counter antimicrobial resistance has taken the serious attention of scientists and clinicians. For example, AgNPs (Burda et al., 2005; Morones et al., 2005) offer a viable alternative to treat infections caused by multidrug-resistant (MDR) microorganisms (Franci et al., 2015; Rai et al., 2009) due to their broad-spectrum and potent antimicrobial properties (Radzig et al., 2013). Silver is considered to be a Lewis acid, which tends to react with a Lewis base, including phosphorous- and sulfur-containing biomolecules that belong to the cell membrane, proteins, and DNA bases (Wiley et al., 2005; Dakal et al., 2016; Ansari et al., 2014; Sondi et al., 2004). Ag-NPs initially accumulate on the cell wall and cell membrane, resulting in morphological changes such as shrinkage of the cytoplasm, membrane detachment, numerous electron-dense pits, and cell membrane disruption (Sondi et al., 2004). In this study, three types of monometallic, bi-metallic, and trimetallic (AgNPs, AuNPs & PdNPs) were synthesized using 3-GPTMS, cyclohexanone, and formaldehyde as reducing agents while, 3-APTMS stabilized the

nanoparticle physical properties followed by antibacterial activity evaluation against multi-drug resistant *Acinetobacter baumannii* and conducted the preliminary investigation on protein–nanoparticle interactions at cell surface using fluorescence spectroscopy.

2.2 Experimental

2.2.1. Materials

3-aminopropyltrimethoxysilane (3-APTMS), 3-glycidoxypropyltrimethoxysilane (3-GPTMS) chloroauric acid trihydrate ($HAuCl_4.\ 3H_2O$), Bovine serum albumin (BSA) and silver nitrate ($AgNO_3$) were obtained from Aldrich Chemical Co. (Bengaluru, India). Bacterial culture media such as Muller–Hinton Broth (MHB), Muller–Hinton Agar (MHA), Nutrient Agar (NA) and Nutrient Broth (NB) were purchased from Hi-Media Laboratories Ltd. (Mumbai, India). Plastic wares were purchased from Tarson Product Pt. Ltd. (Kolkata, India). The antibiotics and other routine chemicals were purchased from Sigma Aldrich Inc. (St. Louis, MO, USA). The organic solvents used were obtained from Merck Millipore (Merck Life Science Private Limited, India). All of the reagents were of analytical grade.

2.2.2. Bacterial strain

We isolated one strain of *A. baumannii* from the endotracheal tube secretions of one intensive care unit (ICU)-admitted male patient who had developed ventilator-associated pneumonia. This strain was identified based on the culture characteristics of MacConkey agar and blood agar, Gram staining, and biochemical tests such as catalase, oxidase, sugar fermentation, and citrate utilization. On antibiotic susceptibility testing, this strain was only sensitive to polymyxin B; it showed resistance to the other tested antibiotics, including amoxicillin–clavulanic acid, ceftazidime, gentamycin, amikacin, ciprofloxacin, levofloxacin, ampicillin–sulbactam, piperacillin–tazobactam and the carbapenem group of antibiotics.

2.2.3. Synthesis of alkoxysilane functionalized noble metal (mono-, bi-, and tri-metallic) nanoparticles

The noble metal mono-, bi-, and tri-metallic nanoparticles were synthesized from 3-APTMS capped silver, gold, and palladium cations in the presence of three different organic reducing agents, specifically (i) cyclohexanone, (ii) 3-GPTMS and (iii) formaldehyde.

2.2.3.1 3-APTMS and cyclohexanone mediated synthesis of Ag-NP-1 nanoparticles

Ethylene glycol di-acetate (120 µL) and a methanolic solution of 1-vinyl 2-pyrrolidone (540 mM, 100 µL) were placed in a 2mL glass vial, followed by the addition of a methanolic solution of $AgNO_3$ (10 mM, 10 µL), 3-APTMS (150 µL) of the desired concentration (0.5–5M) and cyclohexanone (20 µL). The reaction mixture was thoroughly mixed on a vertex mixture for 30 seconds and processed in a microwave for 15 seconds. The microwave processing cycle was repeated 3 to 5 times, resulting in the appearance of a deep yellow color that indicated the formation of AgNP-1.

2.2.3.2 3-APTMS and 3-GPTMS-mediated synthesis of AgNP-2 nanoparticles

Ethylene glycol di-acetate (120 µL) and a methanolic solution of 1-vinyl 2-pyrrolidone (540 mM, 100 µL) were placed in 2mL glass vial, followed by the addition of a methanolic solution of $AgNO_3$ (10 mM, 10 µL), 3-APTMS (150 µL) and 3-GPTMS (2 M, 350 µL). The reaction mixture was thoroughly mixed on a vertex mixture for 30 seconds and processed in a microwave for 15 seconds. The microwave processing cycle was repeated 5–8 times, resulting in the appearance of a deep yellow color that indicated the formation of AgNP-2.

2.2.3.3 3-APTMS and formaldehyde-mediated synthesis of Ag-NP-3 nanoparticles

Ethylene glycol di-acetate (120 µL) and a methanolic solution of 1-vinyl 2-pyrrolidone (540 mM, 100 µL) were placed in a 2mL glass vial, followed by the addition of a methanolic solution of $AgNO_3$ (10 mM, 10 µL), 3-APTMS (150 µL), and formaldehyde (12 µL). The reaction mixture was thoroughly mixed on a vertex mixture for 30 seconds and processed in a

microwave for 15 seconds. The microwave processing cycle was repeated 2–3 times, resulting in the appearance of a deep brown color that indicated the formation of AgNP-3.

2.2.3.4 3-APTMS and cyclohexanone mediated synthesis of AuNP-1 nanoparticles

Ethylene glycol di-acetate (100 µL) and a methanolic solution of $HAuCl_4$ (25 mM; 100 µL) were placed in a 2mL glass vial, followed by the addition of a methanolic solution of 3-APTMS (150 µL) and cyclohexanone (200 µL). The reaction mixture was thoroughly mixed on a vertex mixture for 30 seconds and processed in the microwave for 15 seconds. The cycle was repeated 2–3 times in a microwave, resulting in the appearance of a deep pink color that indicated the formation of AuNP-1.

2.2.3.5 3-APTMS and 3-GPTMS-mediated synthesis of AuNP-2 nanoparticles

Ethylene glycol di-acetate (120 µL) and methanolic solution of $HAuCl_4$ (25 mM, 100 µL) were placed in a 2mL glass vial. A methanolic solution of 3-APTMS (150 µL) and 3-GPTMS (100 µL) was added to this mixture. The reaction mixture was thoroughly Mixed on a vertex mixture for 30 seconds and processed in a microwave for 15 seconds. The cycle was repeated 3–5 times in the microwave. The mixture showed a deep pink color, indicating the formation of AuNP-2.

2.2.3.6 3-APTMS and cyclohexanone mediated sequential synthesis of Ag–Au–NP-1 bimetallic nanoparticles

Silver nanoparticles were synthesized as described above and diluted eight-folds in methanol. 100 µl of diluted Ag-NPs were mixed with a methanolic suspension of $HAuCl_4$ (100 µl, 25 mM), followed by the addition of cyclohexanone (200 µL), vortex mixing for 30 s, and processed in a microwave for 15 seconds. The microwave processing cycle was repeated 3–4 times.

2.2.3.7 3-APTMS and 3-GPTMS-mediated simultaneous synthesis of Ag–Au–NP-2 bimetallic nanoparticles

Ethylene glycol di-acetate (120 µL) and a methanolic solution of 1-vinyl 2-pyrrolidone (540 mM, 100 µL) were placed in 2mL glass vial, followed by the addition of a methanolic solution of $AgNO_3$ (10mM, 10 µL) and $HAuCl_4$ (25 mM, 100 µL), 3-APTMS (150 µL) and 3-GPTMS (2 M, 350 µL). The reaction mixture was thoroughly mixed on a vertex mixture for 30 seconds and placed in a microwave for 15 seconds. The microwave processing cycle was repeated 5–8 times, resulting in the appearance of a deep reddish color that indicated the formation of Ag–Au bimetallic nanoparticles.

2.2.3.8 3-APTMS and cyclohexanone sequential synthesis of Pd–NP and Pd–Ag bimetallic nanoparticles

120 µl of ethylene glycol di-acetate was placed in a vial. A methanolic solution of $PdCl_2$ (50 µl, 10 mM) was added; the mixture was mixed in a cyclomixer for 30 s. 3-APTMS (100 µl) was mixed into the mixture, followed by formaldehyde (50 µl). The reaction mixture was processed in a microwave for 60 seconds (4 cycles of 15 s). The appearance of black color was associated with the formation of Pd nanoparticles. A five-fold dilution of Pd nanoparticles (200 µL) was placed in a vial, followed by the addition of $AgNO_3$ (10mM, 10 µL); the mixture was mixed in a cyclomixer for 30 seconds. 20 µL of cyclohexanone was added to the mixture and vortexed. The reaction mixture was processed in a microwave and operated for 3–4 cycles of 15 seconds.

2.2.3.9 Sequential Synthesis of Pd–Ag–Au trimetallic Nanoparticles

Pre-synthesized Pd–Ag bi-metallic NPs were diluted 10-fold in methanol. After dilution, 100 µL of diluted NPs were dispensed in a vial, followed by a methanolic solution of $HAuCl_4$ (25 mM, 100 µL). Cyclohexanone was added (200 µL); the reaction mixture was processed in a microwave for 15 seconds (4–5 cycles).

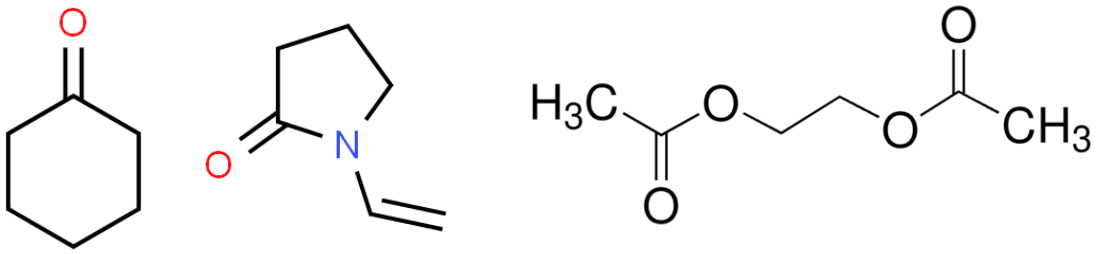

Scheme 2.2. Chemical structure of cyclohexanone, 1-vinyl 2-pyrrolidone, and ethylene glycol diacetate respectively.

2.2.3.10 Characterization of Functionalized Metal Nanoparticles

The mono, bi-, and tri-metallic nanoparticles were characterized using a U-2900 UV-vis spectrometer (Hitachi, Tokyo, Japan) over the scan range from 250 to 800 nm. Transmission electron microscopy analysis and selected area electron diffraction (SAED) were performed using a Techni G2 20 Twin instrument (FEI, Hillsboro, Oregon) at the IIT (BHU) Central Instrumentation Facility (CIF). Samples were made by diluting the nanoparticles in methanol and drop-casting the solution on a carbon-coated copper grid of 300 mesh. Zeta potential analysis was performed in a Zetasizer instrument (Malvern Panalytical, Malvern, United Kingdom). Scanning electron microscopy imaging was performed using an EVO instrument (Carl Zeiss Microscopy GmbH, Jena, Germany) in the CIF.

2.2.3.11 Assessment of antibacterial activity

The antibacterial activity of the synthesized nanoparticles against *A. baumannii* was assessed using the agar well diffusion method. The MIC and MBC values of the nanoparticles were assessed using a two-fold serial dilution method. The MIC value was determined as the minimum concentration at which no turbidity was observed. The MBC value was determined as the minimum concentration at which no bacterial growth was observed on an MHA plate.

2.2.3.12 Assessment by agar well diffusion method

As described previously, AgNP-1, AgNP-2, and AgNP-3 were assessed for antibacterial activity (Poletto et al., 2005). An overnight grown culture of *A. baumannii* in Muller–Hinton broth (MHB) medium was centrifuged; the pellet was inoculated in freshly prepared sterilized MHB medium and incubated for 4 h at 37 ^{0}C. After incubation, a 0.5 MacFarland standard of the bacterial strain containing 0:5x10^8 CFU/mL was prepared (MacFarland, 1907). A sterilized cotton swab spread these cells on freshly prepared MHA plates; the plates were kept undisturbed for 10 min under laminar flow. The wide mouth of sterilized 200 µl micropipette tips was used to make wells on the swabbed plates. All three synthesized nanoparticles were diluted two-fold in 1% DMSO; 20 µl of each nanoparticle was poured into the preformed wells. The same volume of respective test controls (without AgNP-1, AgNP-2, or AgNP-3) was poured in predetermined wells; polymyxin B sulfate and 4% DMSO were also poured in corresponding wells as positive and negative controls, respectively. After pouring each Ag-NPs and control sample, plates were kept undisturbed for 15 min under aseptic conditions for uniform spherical diffusion of the Ag-NPs and controls. The assay plates were incubated at 37 ^{0}C in an incubator for 24 h, followed by observation of any zone of inhibition. All of the experiments were performed in triplicate, and the mean zone of inhibition was measured.

2.2.3.13 Minimum inhibitory concentration (MIC) and minimum bactericidal concentration (MBC).

The minimum inhibitory concentration (MIC) and minimum bactericidal concentration (MBC) of the nanoparticles against *A. baumannii* were determined by using the broth microdilution method in a flat bottom, sterile, 96-well microtiter plate as described previously (Liu et al., 2014). In short, an overnight grown culture of *A. baumannii* in MHB medium was centrifuged and pelleted, followed by re-suspension in fresh MHB medium for 4 h to achieve log phase growth. Further, 0.5 McFarland bacterial suspension containing 0:5 x 10^8 cfu/mL was

maintained. A working suspension of 112 µg/mL of each AgNP was prepared in 4% DMSO; 100 µl of the suspension was placed in each well in a double dilution concentration ranging from 0.43 to 112 µg/ml. 100 µL of 0.5 McFarland bacterial suspension was then added to each well. Test control (without AgNPs), one bacterial control (without treatment), positive control with polymyxin B, and negative control with only media solution were evaluated. The microtiter plate was incubated at 37 ^{0}C for 24 h and observed visually for growth inhibition, which was considered the MIC. Subsequently, five µl of suspension from each well was inoculated on the MHA plates and observed for growth. The MBC was determined as the concentration at which no growth was observed after 24 h of re-incubation.

2.2.3.14 Time kill assay

An overnight grown culture of *A. baumannii* in MHB was centrifuged, and pellets were re-suspended in MHB medium for 4 h at 37 ^{0}C to achieve the log phase of growth. 100 µl of each AgNP at their respective MBC concentration and control were dispensed in a 96-well, flat bottom, sterile polystyrene microtiter plate. Subsequently, 100 µl of 0.5 MacFarland standard of *A. baumannii* suspension was poured into each well and incubated at 37^{0}C in a shaker incubator. Further, 5 µl of culture from each well was spread on MHA plates at different time intervals (0, 1, 2, 4, 6, 8, 12, and 24 h) and incubated overnight at 37^{0}C to determine the viable bacterial count values.

2.2.3.15 Dose-dependent kill kinetic analysis

A time-kill assay was conducted, which involved understanding the effects of AgNP-1, AgNP-2, and AgNP-3 from 1.75 to 56 µg/mL on *A. baumannii*. Data was collected after 6 h of exposure followed by spread over the MHA plate, and the surviving cells were counted; the killing percentage was calculated using the following formula (Chen et al., 2003)

$$\textit{Percent cell reduction} = \frac{(A-B)\times 100}{A}$$

In this equation, A is the number of viable cells before treatment, and B is the number of viable cells after treatment. The dose-dependent kill curve graph was plotted using Graph Pad Prism version 8.2.1 software.

2.2.3.16 Scanning Electron Microscopy

An overnight grown culture was inoculated in fresh MHB medium for 4 h to achieve the log phase of culture; the log phase culture was adjusted to 10^8 cfu/mL in fresh MHB medium and treated with each nanoparticle type for 1 h at 37^0C in a shaker incubator. The cells were then harvested using centrifugation at 3500 rpm for 8 min; the pellet was suspended in 0.1M phosphate buffer (pH=7.2), followed by centrifugation. The pellet was suspended in 2.5% glutaraldehyde solution for 30 min and again centrifuged; the pellet was washed with phosphate buffer followed by centrifugation. The washed pellet was suspended in 1% OsO_4 in phosphate buffer for 45 min and washed with phosphate buffer; the cells were dehydrated with 35%, 50%, 75%, 95%, and 99% ethanol each for 15 min. The dehydrated cells were dried in a vacuum desiccator overnight and coated with gold before scanning electron microscopy imaging.

2.2.3.17 Fluorescence Spectroscopic Studies

2D fluorescence spectra and 3D fluorescence imaging of log phase *A. baumannii* cells (10^4 CFU/mL) grown in nutrient broth and treated with nanoparticles were studied in ultra-pure sterilized water under at 37^0C for 15 min in a Hitachi 7000 fluorescence spectrophotometer (Hitachi, Tokyo, Japan) with excitation and emission matrix at 280 nm and 300 nm, respectively. A scan range of 300–500 nm was used in this study. Bovine serum albumin was chosen as the standard protein to understand the process of nanoparticle-protein interaction;

2D and 3D fluorescence spectra of bovine serum albumin in the absence and the presence of AgNP-1 nanoparticles were recorded (Mariam et al., 2011).

2.3. Results

2.3.1. 3-APTMS-mediated rapid synthesis of noble metal monometallic, bimetallic, and trimetallic nanoparticles

3-aminopropyltrimethoxysilane acts as a Lewis acid to facilitate interactions with metal cations and serves as a potential stabilizer for many metal nanoparticles. 3-aminopropyltrimethoxysilane-treated metal cations initiate the opening of the epoxide ring of 3-GPTMS, forming a covalent linkage with the nitrogen of the amine linked to tri alkoxysilane; this approach results in the reduction and stabilization of the noble metal cations and enables the synthesis of noble metal nanoparticles. This reaction scheme allows control over the reduction process of noble metal cations and enables various combinations of bimetallic and trimetallic noble metal nanoparticles to be produced. In addition, the ratio of amino tri alkoxysilane- and glycidyl-linked tri-alkoxysilane controls the dispersibility in desired polar and nonpolar solvents. Organic aldehydes and ketones may also control the nanoparticle synthesis process. We previously demonstrated that 3-APTMS-treated noble metal cations could be converted into monometallic, bimetallic, and trimetallic nanoparticles (Pandey & Chauhan, 2012; Pandey et al., 2014 a; Pandey & Pandey, 2014 b; Pandey & Pandey, 2016; Pandey & Singh, 2015) however, the time course for the formation of the nanoparticles is approximately 1–8 hours have a function of the type of organic reducing agent (e.g., 3-GPTMS, cyclohexanone or formaldehyde). Since the alkoxysilane and the organic reducing agent are active under microwave irradiation, we sought to understand the role of microwave processing in the functional alkoxysilane-assisted synthesis of nanoparticles. Interestingly, the time required for the conversion of noble metal cations into nanoparticles was reduced to the order

of 15–45 s under microwave irradiation in the presence of an organic reducing agent (e.g., 3-GPTMS, cyclohexanone, or formaldehyde). The formation of monometallic gold nanoparticles, palladium nanoparticles, Ag–Au, Au–Pd bimetallic nanoparticles, and Ag–Au–Pd trimetallic nanoparticles was demonstrated. Figure 2.1 shows the formation of monometallic gold nanoparticles within less than 1 min in the presence of 3-APTMS with cyclohexanone (Figure 2.1(A) (i)–(iii)) and 3-APTMS with 3-GPTMS (Figure 2.1(B) (i)–(iii)). The maximum absorbance between 519–530 nm indicates that gold nanoparticle formation within less than 1 min was demonstrated (Figure 2.1(i)). The average size of gold nanoparticles was < 10nm in each case. Notably, an optimum concentration of 3-APTMS with an organic reagent like cyclohexanone and 3-GPTMS allowed the maximum conversion of metal cations into respective nanoparticles.

This process also enables the formation of silver-gold bimetallic nanoparticles under similar conditions. Figure 2.2 (A) (i)–(iii) shows the characterization data from Ag-Au-NP-1 bimetallic nanoparticles made by the reduction of 3-APTMS-treated noble metal cations in a sequential mode. Figure 2.2 (B) (i)–(iii) shows characterization data from Ag-Au-NP-2 bimetallic nanoparticles made 3-APTMS and 3-GPTMS-mediated simultaneous synthesis. The formation of bimetallic nanoparticles was also recorded within less than one minute. In addition, this process enables the formation of Pd-Ag-AuNPs trimetallic nanoparticles under similar conditions. Initially, Pd-NPs were made from 3-APTMS-treated palladium cations in the presence of formaldehyde under microwave processing for 1 minute. The Pd-Ag bimetallic nanoparticles, as shown in Figure 2.3, were made via a sequential mode of silver cation reduction in the presence of made Pd-NPs (Figure 2.3(A) (i)–(iii)) within less than 1 minute under microwave processing. As made, bimetallic Pd-Ag nanoparticles were allowed to form Pd-Ag-Au nanoparticles by adding gold cations in the presence of cyclohexanone under similar

conditions used to form bimetallic nanoparticles. The results, as shown in Figure 2.3 (B) (i)–(iii), justify the rapid formation of trimetallic nanoparticles and reveal the potential advantage of functional alkoxysilane in the synthesis of noble metal nanoparticles and their multi-metallic analogs.

2.3.2 Role of 1-vinyl 2-pyrrolidone in the synthesis of Ag-NPs

The role of VPP was evaluated in silver nanoparticle synthesis. In silver NP synthesis, with increasing the conc. Of VPP simultaneously with 3-APTMS and silver cation, the absorbance of NPs increased while the size of NPs was controlled between 5-10 nm. 1M; 3-APTMS, 540 mM VPP is optimum for ultimately reducing 10 mM Ag^{+} cation into Ag-NP. From the spectral observation and TEM characterization, it has two significant roles in synthesizing AgNPs. 1-It acts as a co-reducing and cation-stabilizing agent in a concentration-dependent manner. 2. VPP also has a role in stabilizing NPs and preventing agglomeration.

2.3.3 Role of Ethylene glycol di-acetate in the synthesis of Ag-NPs

Ethylene glycol di-acetate was used @12% v/v in silver nanoparticle synthesis. It has two significant roles in the microwave-assisted synthesis of silver nanoparticles. First, it prevents the vaporization of supporting solvents to some extent during the microwave-assisted reaction, and second, it prevents the agglomeration of NPs and enhances the dispersibility of particles after synthesis. After the addition of that solvent, the dispersibility of nanoparticles increases significantly in the long term; on the other hand, at higher concentrations, it reacted with salts, and a precipitate was formed. However, after the synthesis of NPs, it is dispersible in pure solvent without any visual change (color) and stable for a long duration.

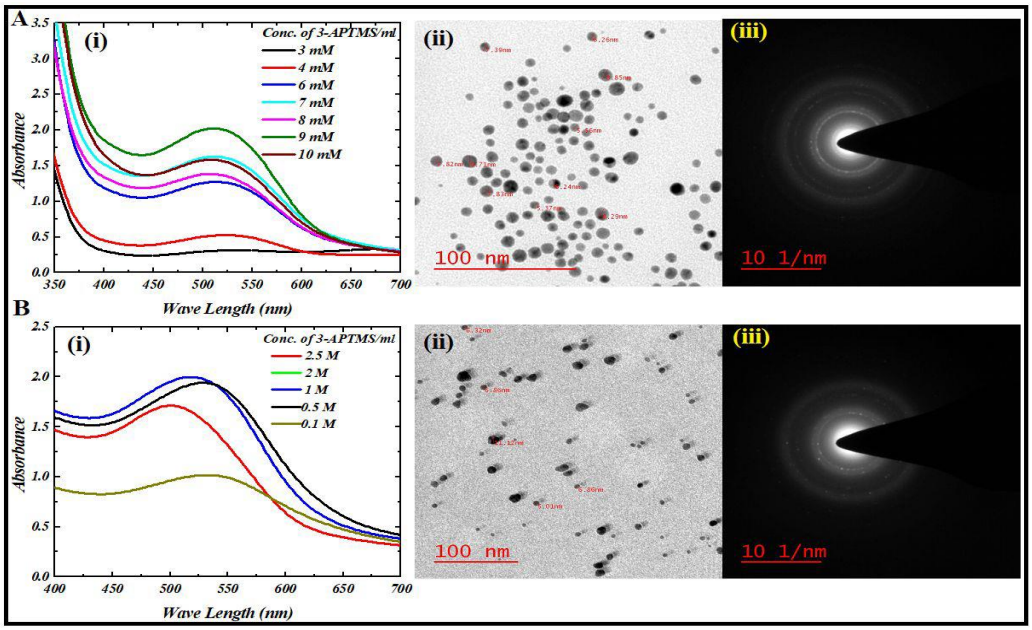

Figure 2.1 (A) Characterization of Au-NP-1 nanoparticles by UV-visible light spectrophotometry (i), transmission electron microscopy imaging (ii), and selected area electron diffraction (SAED) pattern (iii). **(B)** Characterization of synthesized Au-NP-2 nanoparticles by UV-visible light spectrophotometry (i), TEM imaging (ii), and selected area electron diffraction pattern (SAED) (iii).

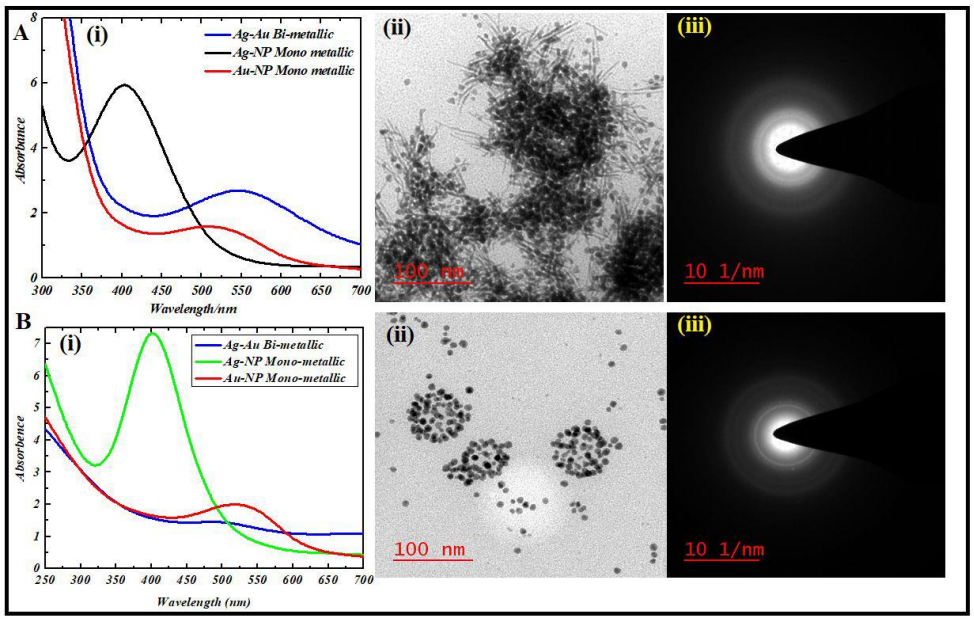

Figure 2.2 (A) Characterization of Ag-Au-NP-1 nanoparticles by UV-visible light spectrophotometry (i), transmission electron microscopy imaging (ii), and selected area electron diffraction pattern (SAED) (iii). **(B)** Characterization of synthesized Ag-Au-NP-2

nanoparticles by UV-visible light spectrophotometry (i), TEM imaging (ii), and selected area electron diffraction pattern (SAED) (iii).

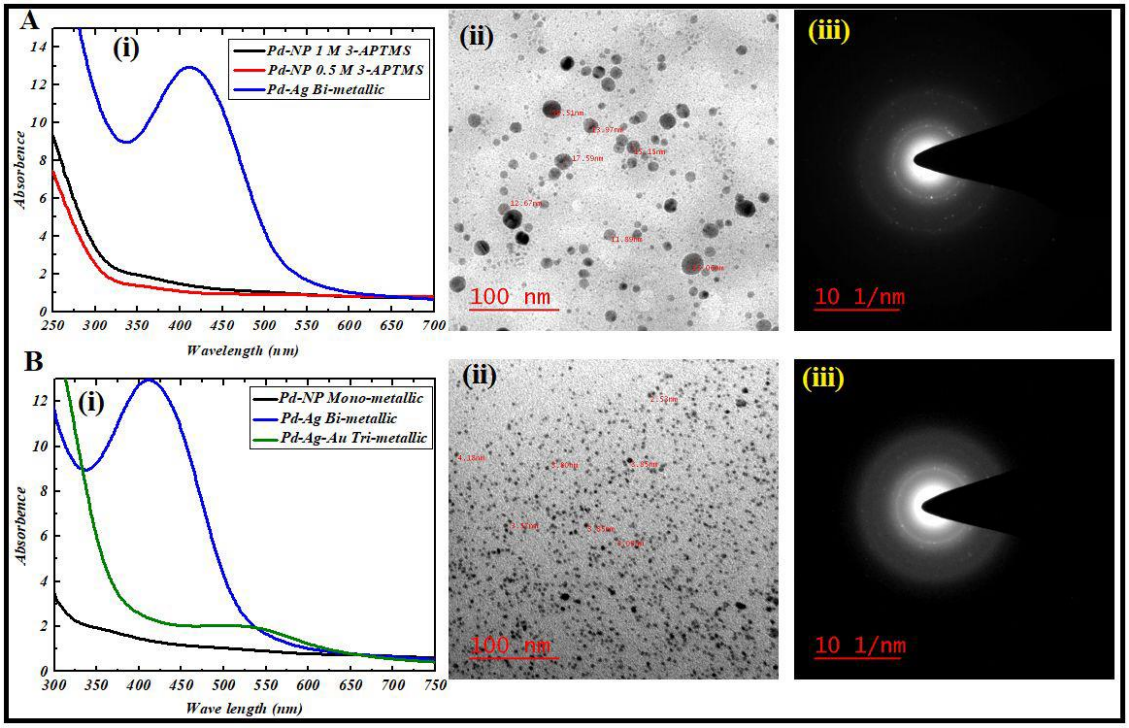

Figure 2.3 (A) Characterization of Pd-Ag bimetallic nanoparticles by UV-visible light spectrophotometry (i), transmission electron microscopy imaging (ii), and selected area electron diffraction pattern (SAED) (iii). (B) Characterization of synthesized Pd-Ag-Au trimetallic nanoparticles by UV-visible light spectrophotometry (i), TEM imaging (ii), and selected area electron diffraction (SAED) pattern (iii).

2.3.4 Antimicrobial activity of noble metal nanoparticles and their multi-metallic analogs.

We attempted to understand the antimicrobial activity of the as-made nanoparticles against *A. baumannii*. The results are shown in Figure 2.4 for Au-NPs (Figure 2.4 i), Pd-Ag-NPs (Figure 2.4 ii), Ag-Au-NPs (Figure 2.4 iii), and Pd-Ag-Au-NPs (Figure 2.4 iv). The zone of inhibition data under similar conditions for the nanoparticles is shown in Figure 2.4 (v). The results indicate that the AuNPs, bimetallic nanoparticles, and trimetallic nanoparticles do not possess significant antibacterial activity; on the other hand, the Pd-NP and Ag-NPs showed

antimicrobial activity (Figure 2.4 v). Since the silver nanoparticles showed potent antimicrobial activity, a detailed investigation of the antimicrobial activity of these particles was performed.

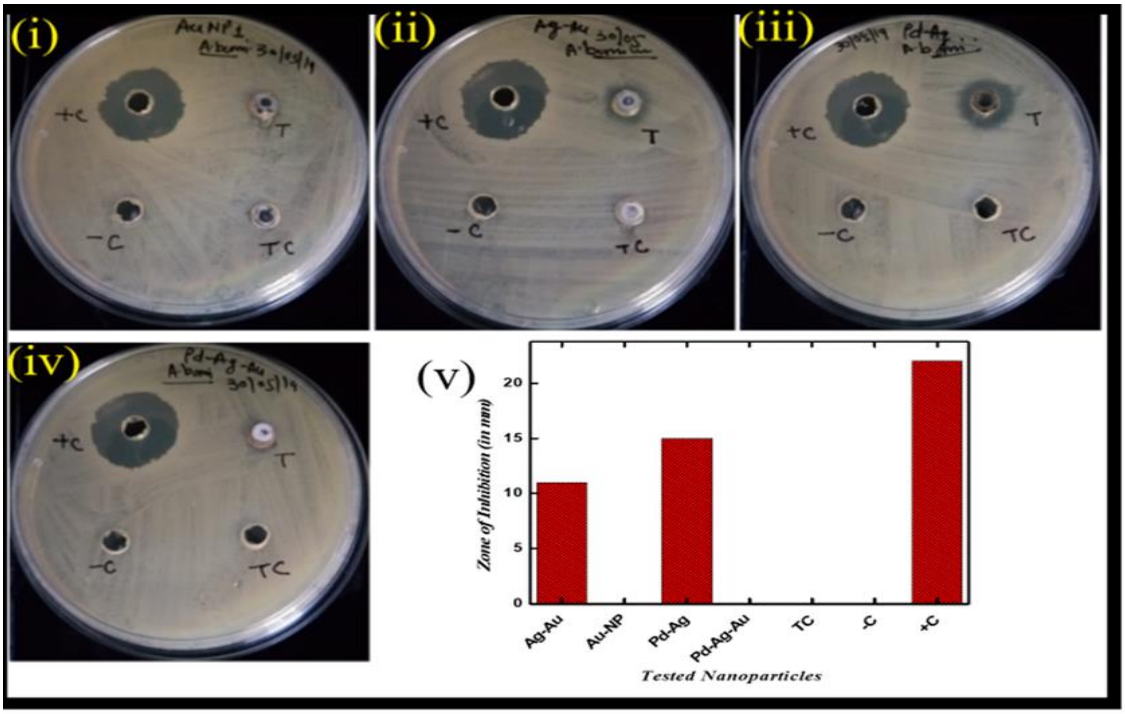

Figure 2.4. Antibacterial assessment plates of bi and tri-metallic nanoparticles against *A. baumannii* by the agar well diffusion method (i-iv), and Zone of inhibition (in mm) (v). TC representing test control (without silver cation).

2.3.5 3-APTMS mediated synthesis of silver nanoparticles as a function of organic reducing agents:

Figure 2.5 A (i) shows the ultraviolet-visible light spectroscopy results recorded from AgNP-1, Figure 2.5 A (ii) shows the ultraviolet-visible light spectroscopy results recorded from AgNP-2, and AgNP-3 shows the ultraviolet-visible light spectroscopy results recorded from AgNP-3. An absorbance maximum of around 405-408 nm has been recorded for all three silver nanoparticles. The TEM and SAED pattern analysis as shown in Figure 2.5 B of Ag-NP-1 (i & iv), AgNP-2 (ii & v), and AgNP-3 (iii & vi); the average size of the AgNP-1, AgNP-2, and AgNP-3 were 9.42, 8.77, and 7.42 nm, respectively. Zeta potential data (Figure 2.5 C) showed

values around 25 mV for AgNP-3 (Figure 2.5 C; iii), indicating higher stability than AgNP-1 and AgNP-2 (Figure 2.5 C; i & ii).

Table 2.1. Physical characteristics of as-prepared mono-, bi-, and trimetallic nanoparticles using 3-APTMS as stabilizing agent and cyclohexanone, 3-GPTMS & formaldehyde as reducing agent.

Nature of Nanoparticles (Stabilizing/reducing agents)	**SPR band (nm)**	**Average size/shape (nm)**	**Zeta potential distribution (mV)**	**Crystal Geometry**
AgNP-1 (3-APTMS/Cyclohexanone)	405	9.42/spherical	~16	FCC
AgNP-2 (3-APTMS/3-GPTMS)	406	8.77/spherical	~18	FCC
AgNP-3 (3-APTMS/Formaldehyde)	408	7.42/spherical	~25	FCC
AuNP-1 (3-APTMS/Cyclohexanone)	520	5.44/spherical	~14	FCC
AuNP-2 (3-APTMS/3-GPTMS)	519	7.22/spherical	~17	FCC
PdNPs (3-APTMS/Cyclohexanone)	NA	12.13/spherical		ND

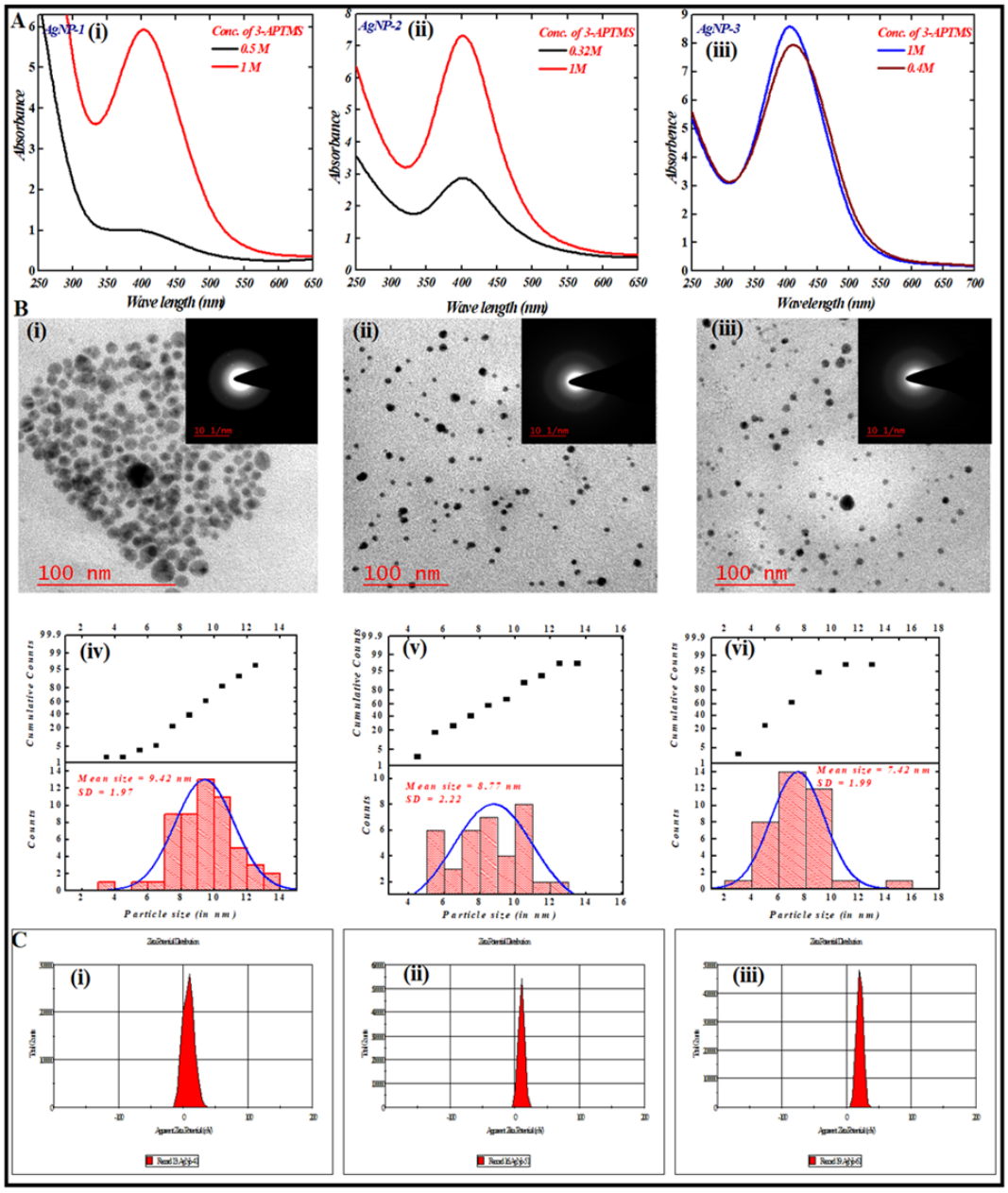

Figure 2. 5 (A) UV-visible light spectrophotometry of AgNP-1 (i), AgNP-2 (ii), and AgNP-3 (iii). (B) Transmission electron microscopy images, a selected area diffraction pattern (inset), and size distribution plots of AgNP-1 (i & iv), AgNP-2 (ii & v), and AgNP-3 (iii & vi). (C) Zeta potential analysis of AgNP-1 (i), AgNP-2 (ii), and AgNP-3 (iii).

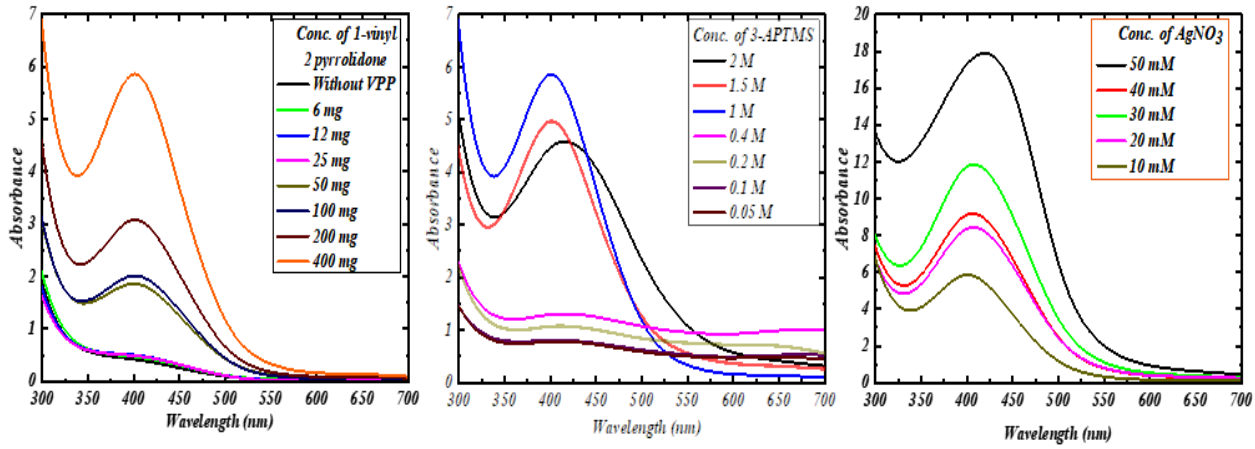

Figure 2.6 Role of variable concentration of 1-vinyl pyrrolidone, 3-APTMS, and silver nitrate on the synthesis of AgNPs.

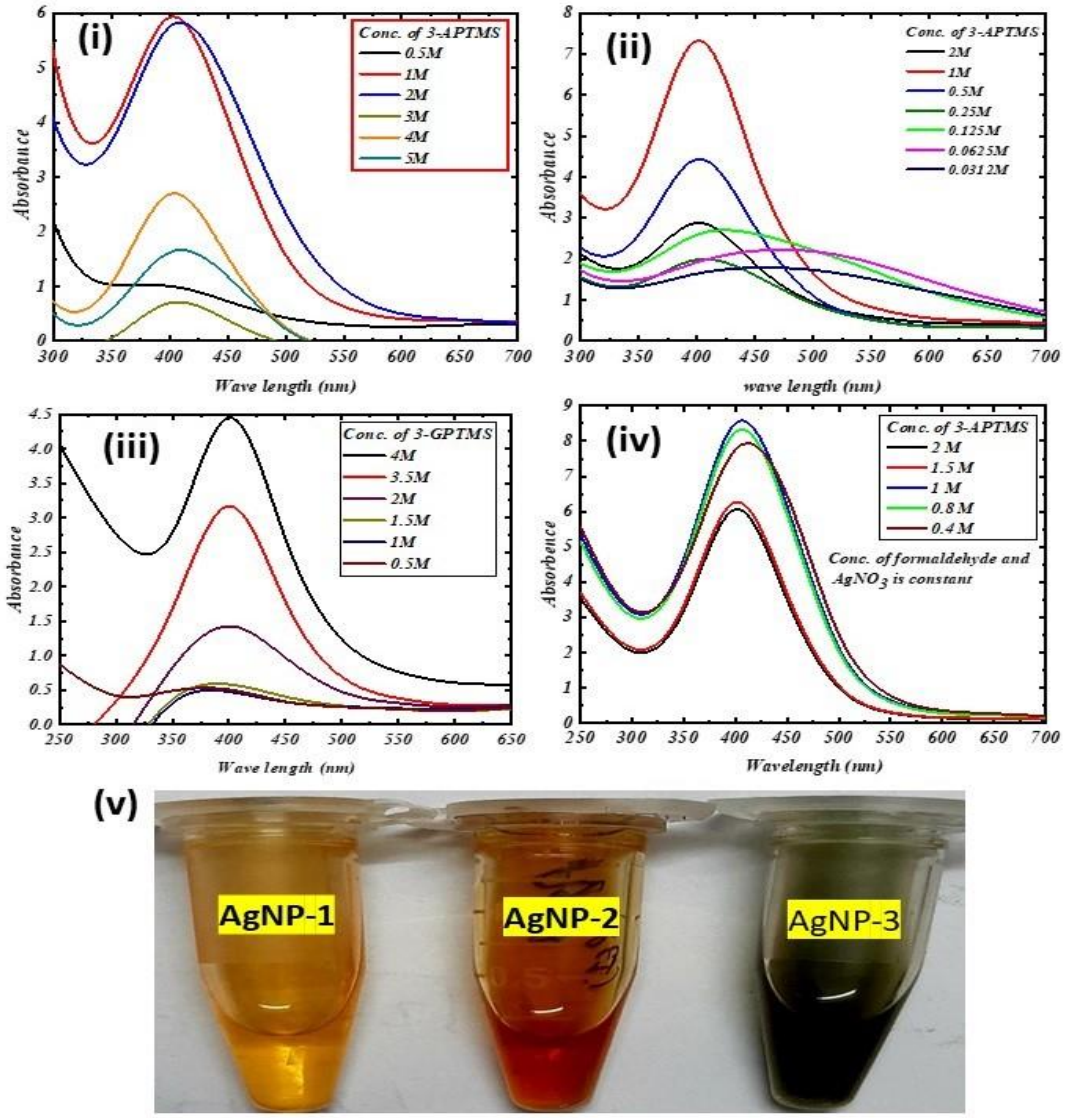

Figure 2.7 Influence of variable concentration of 3-APTMS and 3-GPTMS on LSPR of AgNPs.

Table 2.2. Effect of variable concentration of 3-APTMS/3-GPTMS on the LSPR of silver and gold nanoparticles prepared in methanol under microwave irradiation.

Conc. of 3-APTMS (M)	Conc. of $AgNO_3/Au^{3+}$ (mM)	Volume of Cyclohexanone (µL; v/v)	Absorbance Maxima; SPR (nm)	Absorbance Intensity (a.u.)
AgNP-1; 3-APTMS/Cyclohexanone mediated synthesis				
0.5	10	20	404	1.122
1.0	10	20	409	7.307
1.5	10	20	406	3.132
2.0	10	20	409	6.860
2.5	10	20	421	4.780
3.0	10	20	407	1.020
3.5	10	20	406	3.603
4.0	10	20	407	3.167
5	10	20	412	2.207
AgNP-2; 3-APTMS/3-GPTMS mediated synthesis				
Conc. of 3-APTMS (M)	**Conc. Of $AgNO_3$ (mM)**	**Conc. of 3-GPTMS (M)**	**Absorbance Maxima; SPR (nm)**	**Absorbance Intensity (a.u.)**
0.0312	10	2.5	460	1.284

0.0624	10	2.5	478	2.276
0.125	10	2.5	414	2.935
0.250	10	2.5	406	2.321
0.50	10	2.5	403	5.531
1.0	10	2.5	403	9.378
2.0	10	2.5	408	3.568

AgNP-2; 3-APTMS/3-GPTMS mediated synthesis (3-GPTMS varies)

1	10	0.5	**402**	**0.557**
1	10	1.0	398	0.506
1	10	1.5	405	0.648
1	10	2.0	407	1.697
1	10	2.5	407	1.697
1	10	3.0	408	4.275
1	10	3.5	406	5.710

AgNP-3; 3-APTMS/formaldehyde mediated synthesis

0.4	10	**25**	**413**	**9.536**
0.8	10	25	408	10.418
1	10	25	410	10.773
1.5	10	25	408	8.028

2	10	25	404	7.766

2.3.6 Antimicrobial activity of Ag-NP-1, Ag-NP-2, and Ag-NP-3 against *A. baumannii*

24-hour incubated assay plates were visually examined for the zone of inhibition (ZOI) (Figure 2.7). The assay was performed in triplicate; each ZOI was measured using the zone measurement scale (HI Media, Mumbai, India). All three silver nanoparticles showed a zone of inhibition; the test control (without silver cation) and negative control (4% DMSO) did not show any ZOI (Figure 2.7). Among the three types of silver nanoparticles, AgNP-1 and AgNP-2 showed more potent antibacterial activity than AgNP-3.

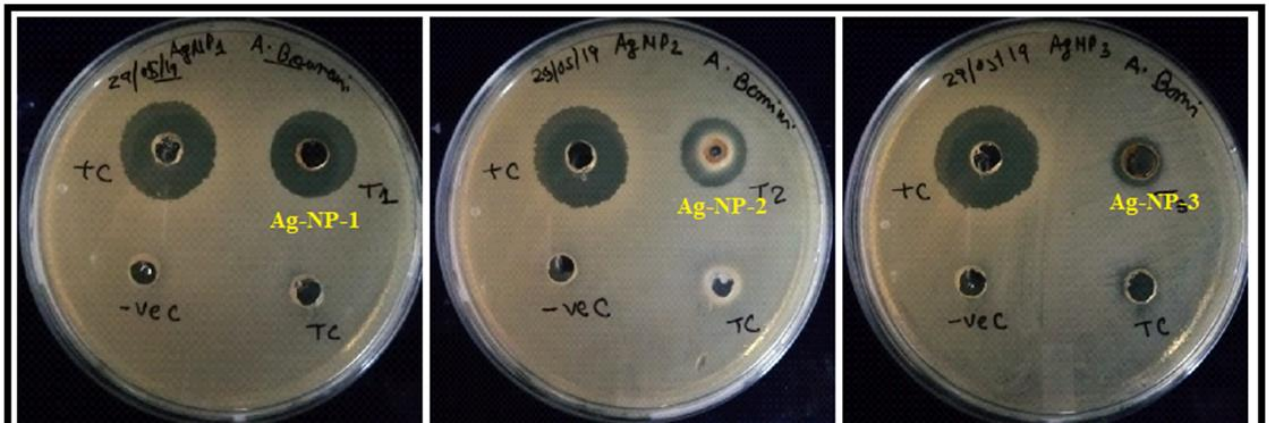

Figure 2.7. Antibacterial assessment plates of AgNP-1, AgNP-2, and AgNP-3 nanoparticles against *A. baumannii* by the agar well diffusion method. TC representing test control (without silver cation).

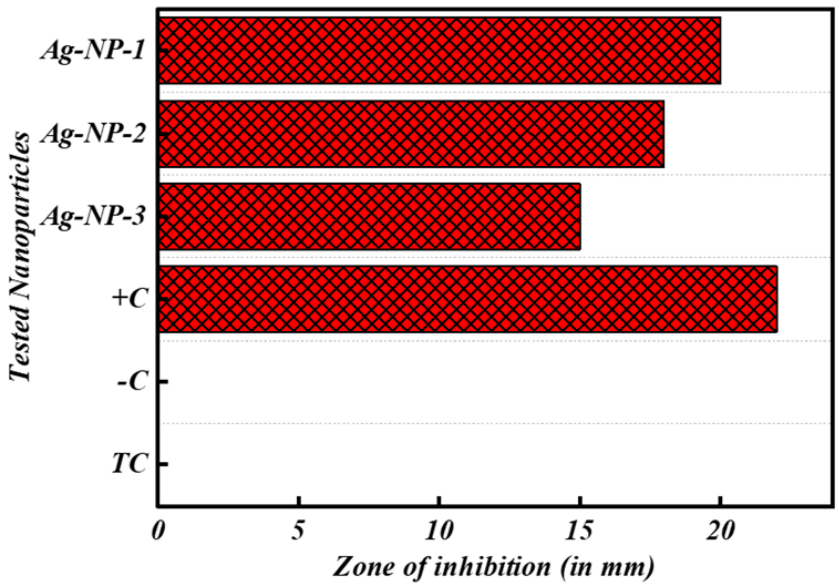

Figure 2.8. Mean zone of inhibition diameter of each type of nanoparticle against *A. baumannii* planktonic cells. +C represents positive control, -C represents negative control, and TC represents test control (without silver cations).

2.3.7 MIC and MBC determination

The MIC and MBC of each silver nanoparticle were determined by the broth microdilution method in flat-bottom, sterile microtiter plates. The MIC of AgNP-1, AgNP-2, and AgNP-3 against *A. baumannii* were 7, 28, and 14 µg/ml, respectively. The MBCs of AgNP-1, AgNP-2, and AgNP-3 against *A. baumannii* were 14, 56, and 28 µg/ml, respectively (Figure 2.8; i). As shown in Figure 2.7, the agar well diffusion assay indicated that AgNP-3 had the lowest ZOI diameter among all of the assessed nanoparticles; however, the MIC and MBC of AgNP-3 were lower than those of AgNP-2.

2.3.8 Time kill assay

A time-kill assay for AgNP-1, AgNP-2, and AgNP-3 was performed at the MIC and MBC levels for these nanoparticles against *A. baumannii*. 5 µL of a bacterial suspension containing the MBC value of each type of silver nanoparticle (14 µg/ml of AgNP-1, 56 µg/ml of AgNP-

2, or 28 µg/ml of AgNP-3) were sub-cultured on MHA plates throughout 0, 1, 2, 4, 6, 8, 12 and 24 hours; no bacterial growth was observed after 6 hours of incubation. A four-log reduction was observed (Figure 2.9; iii) earlier with AgNP-3, followed by AgNP-2 and AgNP-1. Similarly, a time-kill assay at the MIC value of each type of silver nanoparticles was performed (Figure 2.9; ii). A two-log reduction was observed earlier with AgNP-3 than with the two other nanoparticles; final two-log cells remained viable in the suspension at 4 hours with AgNP-3, 6 hours with AgNP-2, and 8 hours with AgNP-1, which persisted even after 24 hours.

2.3.9 Dose-dependent kill kinetics

Dose-dependent kill kinetics was evaluated by counting the surviving bacterial cells after six hours of exposure to double dilution concentration of each type of AgNP. It was shown that 10^2 cfu/ml survived in the medium after exposure to the MIC value of AgNP-1, AgNP-2, or AgNP-3 after six hours of incubation at 37°C. None of the cells survived in the medium after exposure to the MBC value of AgNP-1, AgNP-2, and AgNP-3 after six hours of incubation at 37°C. At lower concentrations (3.5 µg/ml), a one-log reduction was observed for AgNP-1 and AgNP-3; AgNP-2 showed no inhibitory effect (Figure 2.9; iv).

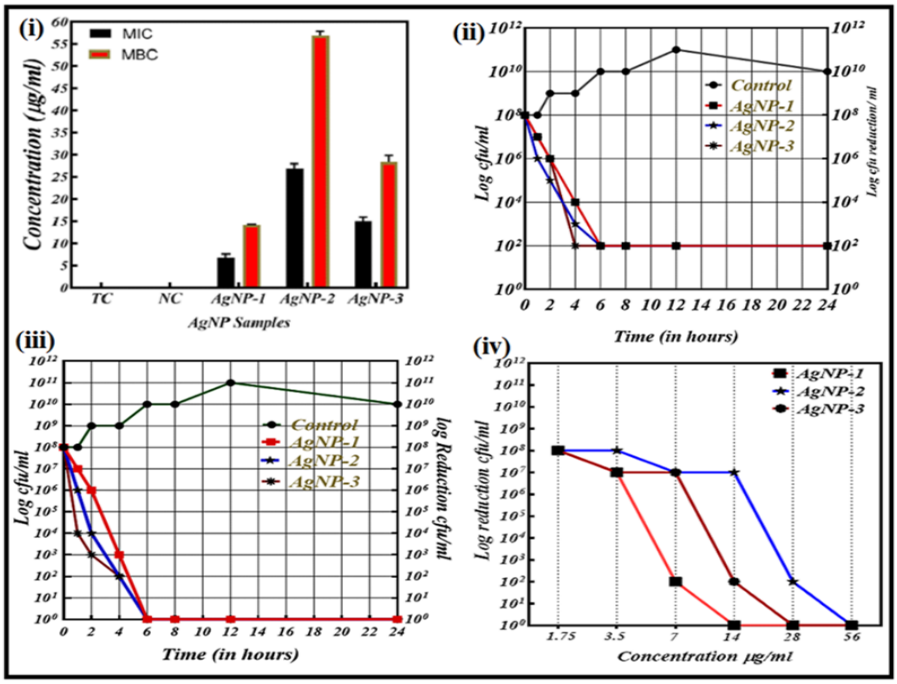

Figure 2.9. (i) MIC (µg/ml) and MBC (µg/ml) values of AgNP-1, AgNP-2, and AgNP-3 against *A. baumannii* planktonic cells. TC represents Test control and NC represents negative control. (ii) Time kill curve of *A. baumannii* with 1x MIC concentration of each nanoparticle at 37^0C under aerobic conditions. Control is represented as untreated cells. (iii) Time kill curve of *A. baumannii* with 1x MBC concentration of each nanoparticle at 37^0C in under aerobic conditions. Control is represented as untreated cells. (iv) The dose-dependent kill curve at different concentrations of AgNP-1, AgNP-2, and AgNP-3 against *A. baumannii* after six hours of treatment at 37^0C under aerobic conditions; log reduction cfu/ml represents the log value of cfu/ml killed at their corresponding concentration (iv).

2.3.10 Scanning electron microscopy analysis

Scanning electron microscopy examination of the silver nanoparticle-treated cells revealed that the silver nanoparticles caused a series of changes in *A. baumannii*, including size and shape alteration as well as bleb formation on the surface (Figure 2.10) within one hour of treatment. AgNP-1 treated cells (Figure 2.10 b) showed a reduction in size with cell fragmentation and bleb formation. AgNP-2 treated cells (Figure 2.10 c) showed cell swelling with cell membrane breakage. AgNP-3 treated cells showed bleb formation, inducing the leakage of intracellular materials (Figure 2.10 d)

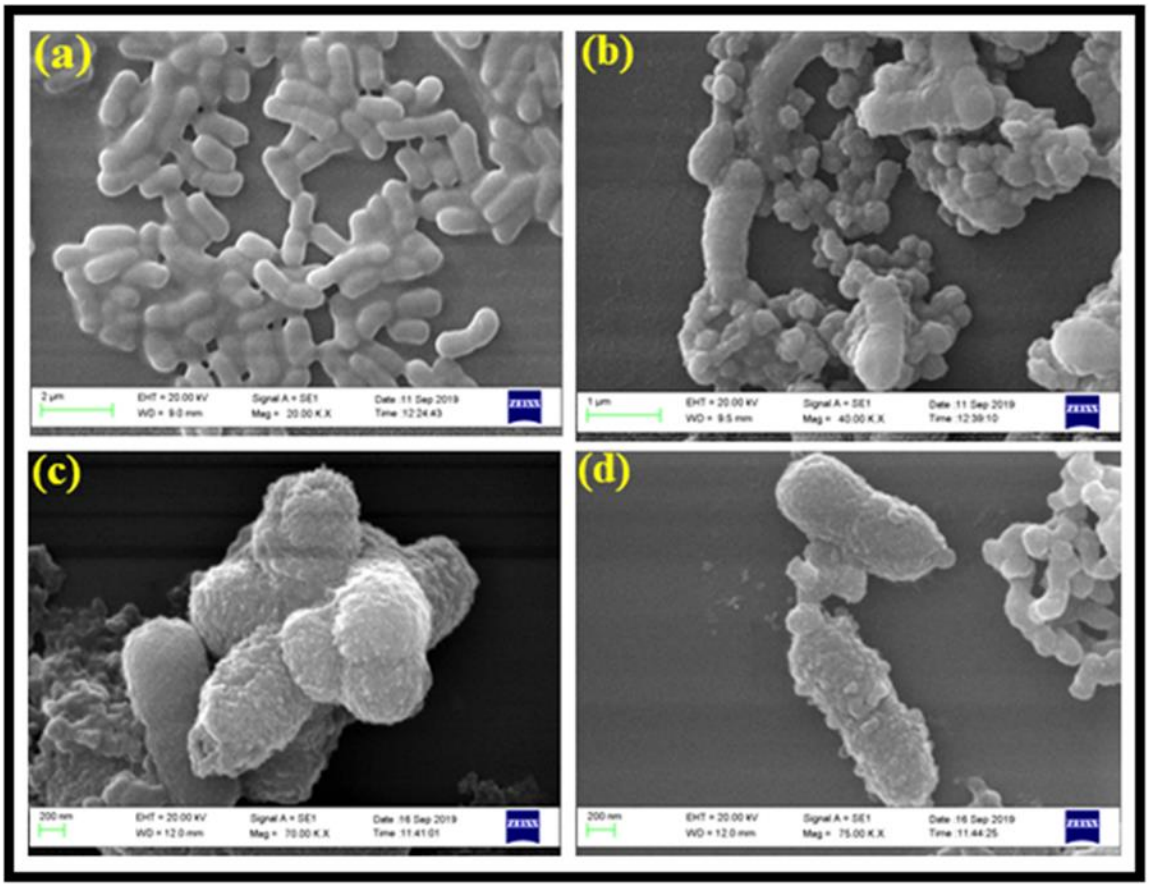

Figure 2.10. Scanning electron microscopy images of control (a), AgNP-1 treated cells (b), AgNP-2 treated cells (c), and AgNP-3 treated cells (d); for 1 hour at respective MIC value in MHB medium at 37^0C.

2.3.11 Fluorescence imaging of silver nanoparticles with *A. baumannii* cell surface. Protein-nanoparticle interactions may be evaluated through fluorescence imaging. Accordingly, we attempted to investigate the interaction of AgNP-1 with bovine serum albumin using 2-D and 3-D fluorescence imaging. Figure 2.11 A shows the 2-D fluorescence spectra in the absence (1) and the presence (2) of AgNP-1. The finding predicts that after Ag-NP-1 interaction, the fluorescence intensity is reduced close to zero, indicating selective binding of the silver nanoparticles to the protein. Similar observations were recorded for the interactions between AgNP-1 and *A. baumannii* (Figure 2.11 B). To understand the mechanism of surface

protein binding to AgNP-1, 3-D fluorescence imaging of similar interactions is recorded as shown in Figure 2.11. Figure 2.12 represents 3D fluorescence images of bovine serum albumin in the absence (A, B) and the presence (A', B') of Ag-NP-1. Images A and A' show the contour images; images B and B's

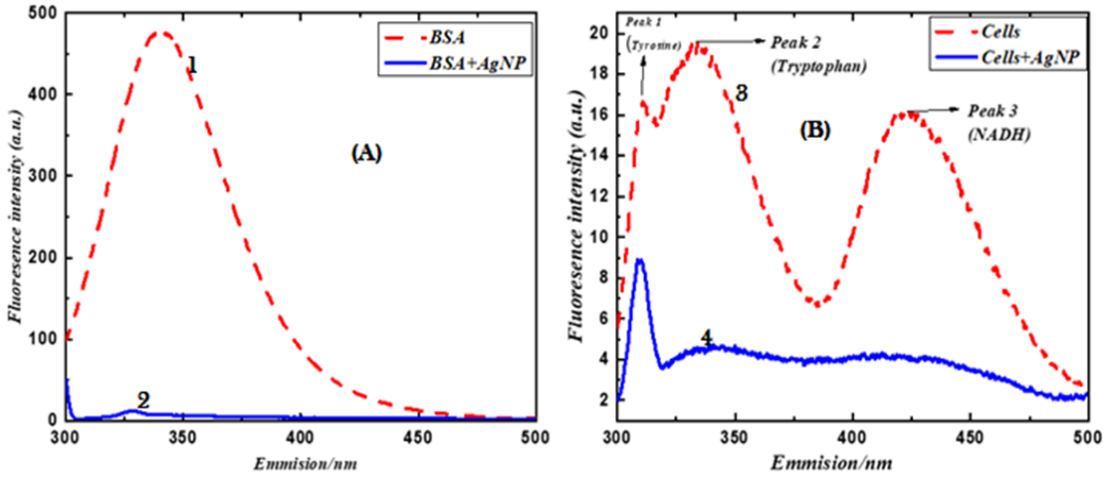

Figure 2.11 (A) Fluorescence spectra of bovine serum albumin in the absence (1) and the presence of AgNP-1 (2). (B) Fluorescence spectra of *A. baumannii* in the absence (3) and the presence of AgNP-1 (4)

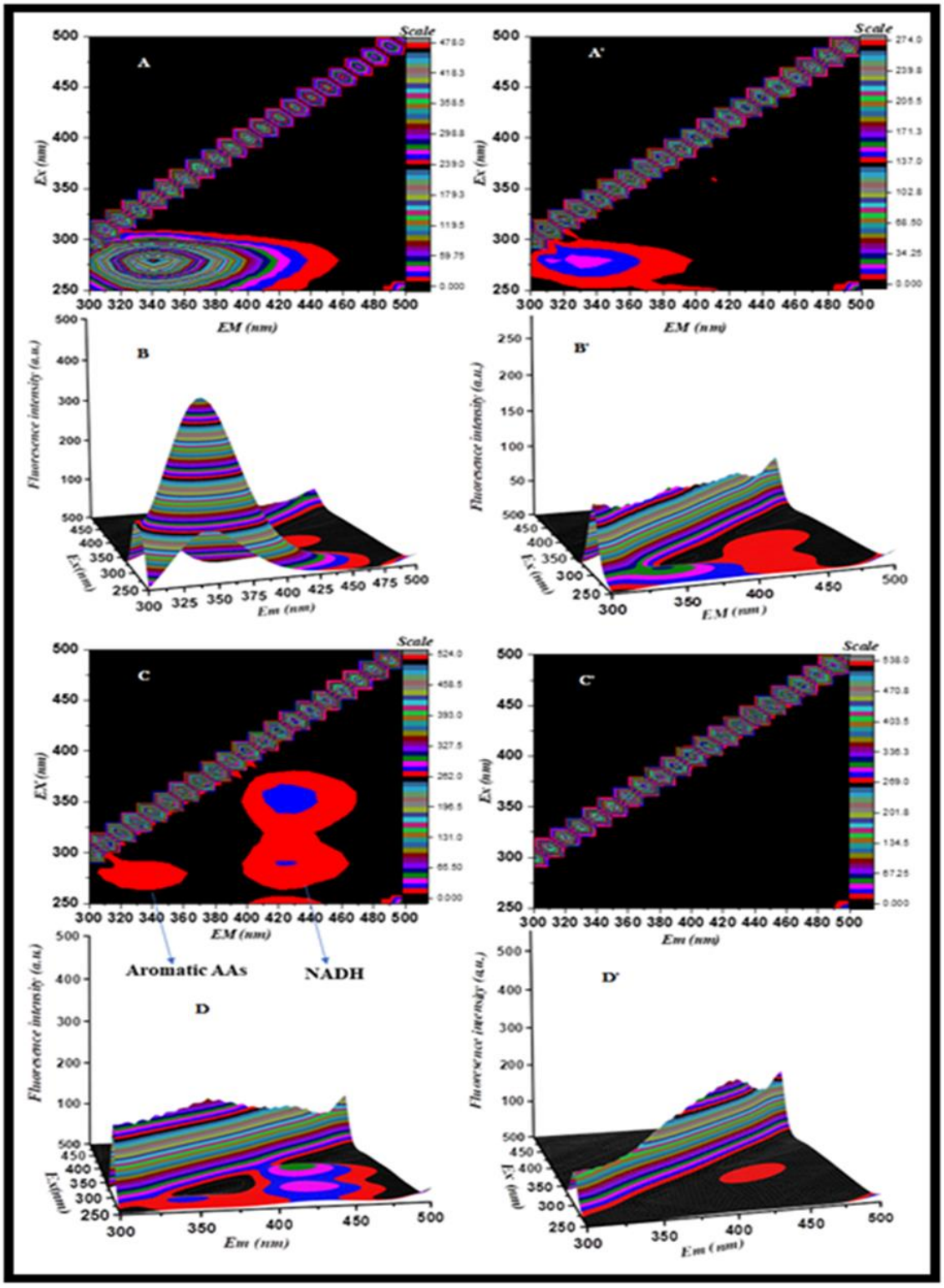

Figure 2.12 3D fluorescence images of bovine serum albumin in the absence (A, B) and the presence (A', B') of AgNP-1. A and A' show the contour images; B, and B' show the surface

images. 3D fluorescence images of *A. baumannii* in the absence (C and D) and the presence (C' D') of AgNP-1. C and D show the contour images; C' and D' show the surface images.

2.2 Discussion

Recently, tri-alkoxysilanes (3-APTMS, 3-GPTMS) stabilized mono-, bi- and trimetallic nanoparticles have been synthesized and successfully explored for various electrochemical sensing applications by Pandey et. al., (Pandey & Chauhan, 2012; Pandey et al., 2014 a; Pandey & Pandey, 2014 b; Pandey & Pandey, 2016; Pandey & Singh, 2015). However, some challenges were associated with synthetic protocols such as long reduction time, stability in aqueous media, and lack of biomedical applications. To overcome such stated challenges, certain modifications are considered i.e., the use of microwave irradiation to fasten the reduction process along with the addition of 1-vinyl 2-pyrrolidone and ethylene glycol diacetate in the reaction mixture to prevent the evaporation of solvent during irradiation and agglomeration. Here, microwave irradiation played a significant role in enhancing the reduction rate of metal cations such as silver, gold, and palladium in the presence of reducing agents such as cyclohexanone, 3-GPTMS, and formaldehyde. Practically, due to the penetrating characteristics of microwaves, homogenous heating of the reaction mixture allowed uniform nucleation, rapid crystal growth, and formation of nano-geometry-controlled crystallites with narrow size distribution. However, the reduction kinetics of metal cations under microwave irradiation are still to be investigated in the presence of tri-alkoxysilanes. Simultaneously, the effect of variable concentrations of 1-vinyl 2-pyrrolidone, and 3-APTMS on nanoparticle synthesis has been examined. The results demonstrated a significant influence of concentration variation on nanoparticles SPR as shown in Figure 2.6 (i). Because 1-vinyl 2-pyrrolidone itself acts as a reducing agent (co-reducing agent in the presented research work), at higher concentration (400 mg/ml) along with cyclohexanone, the absorbance intensity

increased drastically without any shift in SPR attributed to the complete reduction of metal cations and active role in controlling nano-geometry of silver nanoparticles. However, in the case of gold and palladium cations reduction, no significant role was observed at the given parameters. Similarly, the influence of variable concentrations of 3-APTMS on the synthesis of gold and silver nanoparticles was established. The results confirmed the significant role of certain 3-APTMS concentrations in controlling the nano-geometry of gold and silver nanoparticles (≤10 nm) as attributed in Figure 2.6 (ii) & Table 2.2.

Therefore, the antimicrobial behavior of as-prepared mono and multi-metallic analogous nanoparticles was evaluated and investigated against MDR *A. baumminii*. Monometallic; gold nanoparticles, bimetallic; Ag-Au, and trimetallic; Pd-Ag-Au nanoparticles did not demonstrate any significant antimicrobial activity as shown in Figure 2.4. However, 3-APTMS stabilized silver nanoparticles (AgNP-1-3), attributed excellent biocidal activity (Figure 2.7 &8) depending on the functionality of the reducing agent and water dispersibility. Among all AgNPs, AgNP-1 had shown excellent antibacterial activity against tested gram-negative bacteria along with a lower MIC value as demonstrated in Figure 2.9 (i). The rest of all (AgNP-2 & 3) showed narrow activity due to the rapid tendency of polymerization of 3-APTMS in the presence of 3-GPTMS and formaldehyde that ceased the proper water dispersibility, however, prepared nanoparticles had an excellent dispersibility in methanol and DMSO. On the other hand, AgNP-1 (3-APTMS/Cyclohexanone system) was immensely dispersible in water. Further, bacterial surface interaction dynamics of AgNP-1 have been investigated by using fluorescence spectrophotometry, which demonstrated that, nanoparticles quenched the intrinsic fluorescence of bacterial protein suggesting an active interaction of nanoparticles with bacterial surface proteins as shown in Figures 2.11 & 12. This finding was further authenticated by

investigating the surface ultrastructure of bacterial cells as attributed in Figure 2.10 and confirmed the AgNP-1 induced cytostructural damage and ultimately cell death.

Despite being excellent biocidal activity of as-prepared silver nanoparticles, there are some limitations for biomedical applications as the use of a high concentration of 3-APTMS as a stabilizing agent could be a health concern however, the rapid polymerization property of nanoparticle-containing system can be applied as a thin film coating for several medical devices although a rigors experimental optimization and testing required.

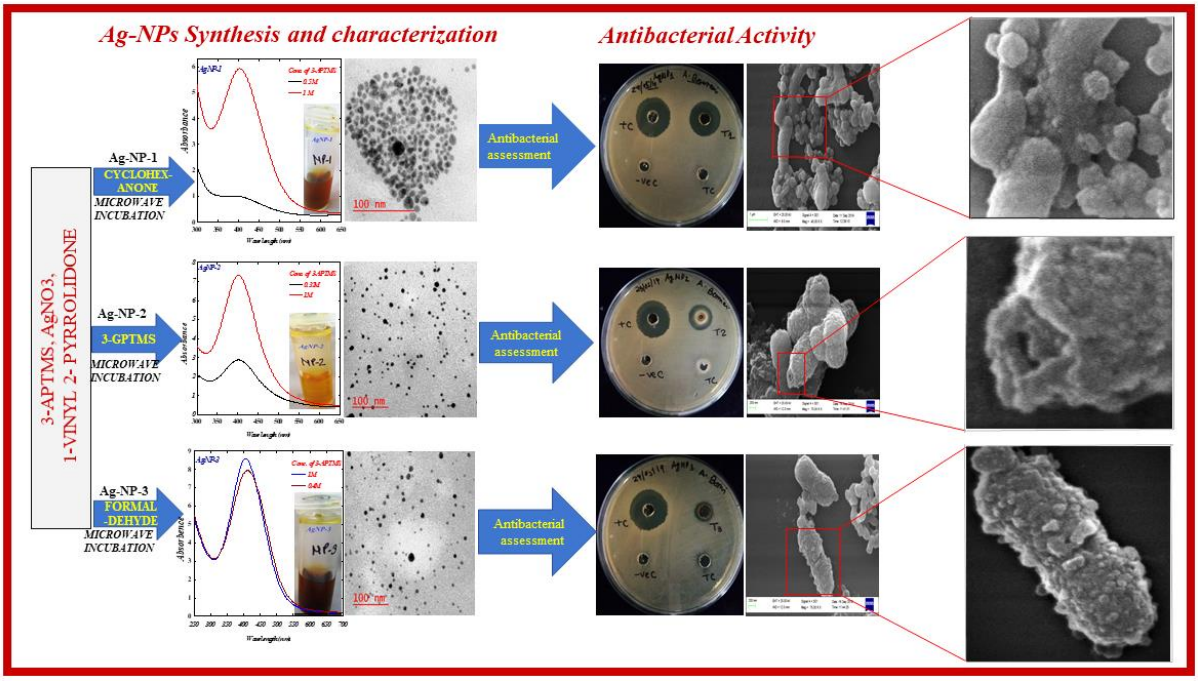

Scheme 2.3 Schematic representation of the chapter's work.

2.3 Conclusion

This chapter describes the organic moiety-dependent rapid synthesis of noble metal mono, bi-,and trimetallic nanoparticles and their antimicrobial activity evaluation against Gram-negative bacteria *Acinetobacter baumminii*. Among all, monometallic (AuNPs), bimetallic (Ag–Au and Pd–Ag), and trimetallic (Pd–Ag–Au) nanoparticles did not show any significant antimicrobial

activity; on the other hand, Pd-NPs and all AgNPs (1-3) were shown to be potent antimicrobial agents. Therefore, AgNPs were chosen for further investigations. AgNPs (1-3) were stabilized with 3-APTMS and reduced with cyclohexanone, 3-GPTMS, and formaldehyde respectively, which allowed the production of three different types of silver nanoparticles, had spherical and less than 10 nm in size, which showed antibacterial properties against a multi-drug resistant *A. baumannii* strain. The MIC and MBC of the AgNP-1 were the lowest among the tested silver nanoparticles due to their hydrophilicity. Further, 2D and 3D fluorescence spectroscopic investigation demonstrated selective cell surface–nanoparticle interactions. The work of presented in this chapter directed us to investigate the dynamics of nanoparticle interaction with the microbial surface (nano-bio interface) and the rational design of novel surface-tuned metal nanoparticles for the delivery of antibiotics and the development of new coating material against deadly nosocomial infections.